

RESEARCH ARTICLE | SEPTEMBER 18 2023

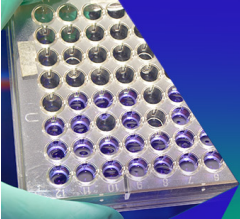
Shock-to-detonation transition behavior of functionally graded energetic materials

Daniel Olsen ; Min Zhou  




J. Appl. Phys. 134, 115901 (2023)

<https://doi.org/10.1063/5.0160553>



Biomicrofluidics
Special Topic:
Microfluidics and Nanofluidics in **India**
Submit Today



Shock-to-detonation transition behavior of functionally graded energetic materials

Cite as: J. Appl. Phys. 134, 115901 (2023); doi: 10.1063/5.0160553

Submitted: 2 June 2023 · Accepted: 25 August 2023 ·

Published Online: 18 September 2023



Daniel Olsen  and Min Zhou 

AFFILIATIONS

The George W. Woodruff School of Mechanical Engineering and The School of Materials Science and Engineering, Georgia Institute of Technology, Atlanta, Georgia 30332-0405, USA

^{a)}Author to whom correspondence should be addressed: min.zhou@gatech.edu

ABSTRACT

The behavior of energetic materials is significantly influenced by the spatial distributions of microstructure heterogeneities and voids. We pursue the concept of Functionally Graded Energetic Materials whose microstructure features (e.g., grain size, grain volume fraction, void size, and void volume fraction) change spatially such that they may allow the behavior of the materials to be tailored. We explore using gradients in the density of voids to alter the detonation behavior of a polymer-bonded explosive (PBX) echoing PBX9501 with HMX (octahydro-1,3,5,7-tetranitro-1,3,5,7-tetrazocine) grains and Estane binder. Five cases, two graded void distributions from 1% to 10% and 10% to 1% by volume along the length of the sample, and three uniform distributions matching the lowest (1%), average (5.5%), and highest (10%) void densities are considered. An Arrhenius reaction burn model is used to account for the chemical kinetics of HMX. Different detonation behaviors are obtained from the same graded sample when impact loading is from 1% void end and from the 10% void end as well as from the uniform cases. The SDT (shock to detonation transition) behaviors are analyzed in terms of the run distance, the time duration and shock velocity changes over the SDT process. The computational results are presented in the context of available experimental data for PBX9501 with which agreement is obtained through a parametric study. Overall, it is shown that gradients in microstructures of PBX can lead to SDT behaviors different or not obtainable from microstructures without gradients, thereby offering a mechanism for designing and tailoring new materials.

Published under an exclusive license by AIP Publishing. <https://doi.org/10.1063/5.0160553>

I. INTRODUCTION

Microstructural heterogeneities have long been understood to have a profound impact on the ignition and detonation of energetic materials through the development of hotspots, which are areas of significant temperature rise.^{1,2} Voids and other microstructure defects, such as cracks, are the most probable sites for hotspots formation.³ Most of these heterogeneities can be very small on the scale of micrometers or nanometers. Understanding the underlying physics of cracks and voids and taking advantage of the trends are of importance in the development of new energetic materials.

Large mesoscale models at overall millimeter macroscopic size scales are capable of explicitly accounting for distributions of both material constituent heterogeneities and voids. In addition, they also explicitly track and resolve the spatial and temporal scales of the shock wave propagation, evolution of chemical reaction, ignition, shock to detonation transition (SDT), and propagation of detonation wave in unshocked material. As such, the primary size

scales of experiments are captured.⁴ A common metric used in the energetics community is the run-to-detonation distance (RDD), which is usually millimeters or centimeters in scale.⁵ The size and density of energetic crystals can vary widely depending on the type of crystal [e.g., HMX (octahydro-1,3,5,7-tetranitro-1,3,5,7-tetrazocine), PETN (pentaerythritol tetranitrate)] and material processing.³ Crystal size and shape can affect the RDD.^{6–9} Baer *et al.*¹⁰ built a cubic millimeter volume with ~1900 grains to understand the shock loading effects. Miller *et al.*⁴ used 3D void explicit microstructure models with sizes up to $3 \times 3 \times 15 \text{ mm}^3$ to analyze the detonation behavior of HMX. Different microstructure combinations were used, including uniform sample without grains, microstructured samples without voids, and corresponding cases with voids. They found that the sensitivity of the material increases with both material heterogeneity and voids.

Coffelt *et al.*¹¹ studied the effects of void positioning relative to the grains and the binder of a PETN/HTPB (hydroxyl-

29 March 2024 19:41:53

terminated polybutadiene) energetic composite. It was found that void placement within just the grains, just in the binder, or in both resulted in different behaviors and the effects of voids in the different types of sites interact, especially at higher shock pressures. These studies have shown that it is now possible to (1) systematically explore the behavior of energetic materials at scales approaching experimental scales and microstructure details that capture primary heterogeneities of interest and (2) delineate trends and underlying mechanisms to understand and pursue the design of material configurations not yet in existence.

Most analyses assume the microstructure heterogeneities are spatially uniform in a statistical sense. However, material synthesis processes can lead to spatially non-uniform distributions of material constituents and defects. For example, Olinger¹² found that the density varies from one end to the other in compressed cylindrical PBX 9501 and 9502 composites. Gharia *et al.*¹³ noted that different sections of a cast energetic composite can have different densities due to sedimentation of larger energetic crystals such that the sections have different sensitivities to shock. Zhang *et al.*¹⁴ showed that grain, and, therefore, overall material density, distributions vary within cast PBX composites. Measures have been taken to control microstructure formation. For instance, Yeager *et al.*¹⁵ found that centrifuging HMX/HTPB composites both reduces void size and leads to more even spatial distribution of voids. Defoaming agents have also been found to be able to control void concentration in PBX.¹⁶ We regard these unintentional or intentional existence of microstructure spatial inhomogeneities as both challenges and opportunities, in the sense that spatial microstructure gradients can be used as a means to modify the material behavior in potentially desirable manners.

Therefore, to further expand the microstructure space for materials design and exploration, we use the concept of Functionally Graded Energetic Materials (FGEMs) or Functionally

Graded Reactive Materials (FGRMs)¹⁷ which have spatially non-uniform or graded microstructures. The idea is to introduce and take advantage of spatial variations in material features such as the size and densities of voids, particles, and grains among others to manipulate the material behavior. Several examples are shown in Fig. 1. Here, the FGEM concept is to manipulate the shock response, hotspot development, reaction initiation/propagation, shock to detonation transition (SDT), and detonation propagation through (i) spatial gradients of material attributes such as high-explosive (HE) crystal size [Fig. 1(a)] and packing density [Fig. 1(b)], voids size and density [Fig. 1(c)], and aluminum particle size and density [Fig. 1(d)]; (ii) sharp interfaces between distinct macromaterial regions [e.g., Figs. 1(e) and 1(f)]; and (iii) combinations of (i) and (ii) and/or other variations. These structural designs are spatially non-uniform, anisotropic, and/or asymmetric, allowing for more dynamic responses. In addition to altering the ignition and detonation behaviors, the samples can also be macroscopically anisotropic or asymmetric; therefore, impacting from different ends can result in different responses of shock propagation, reaction kinetics, SDT, and detonation propagation processes and velocities, thus imparting multifunctionality to each sample.

It is worth point out that this is a theoretical materials design exercise. Although, we are not aware of samples proposed here being made in a laboratory at this time, the development of advanced fabrication techniques will allow the materials proposed in Fig. 1 to be fabricated. Additive manufacturing (AM) techniques such as direct ink writing, electrospray deposition, and stereolithography (SLA) are ideally suited for this task via controlled placement of constituents.^{18–22} Indeed, materials echo the attributes in Fig. 1 have already been made. For example, Zhou *et al.*²³ prepared layered RDX/HTPB composites containing 0% to 30% aluminum. The microstructures are similar to what we propose in Figs. 1(d)–1(f).

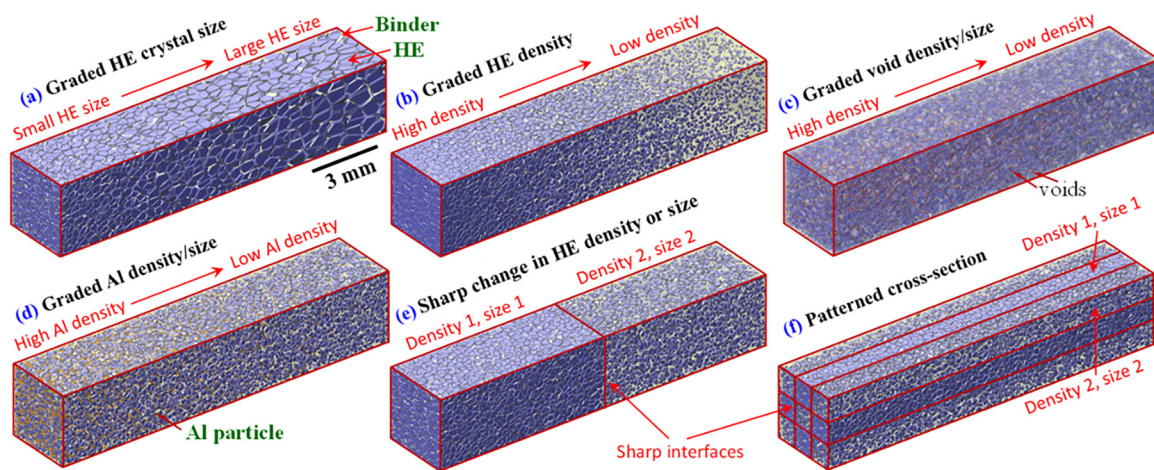


FIG. 1. Examples of candidate designs of functionally graded energetic composites (FGEC). These designs can offer mechanisms for response tailoring. In addition, they are also anisotropic so can be impacted in different directions to obtain different effects. The design approach utilizes gradients in constituent size, density, voids, in-material interfaces, and combinations thereof for shock, initiation, reaction, and detonation behavior tailoring. (a) Gradient of energetic crystal size, (b) gradient of energetic crystal density, (c) gradient of void density and size, (d) gradient of density and size of additional constituents such as aluminum particles, (e) sharp transition in density or size of constituents, and (f) combinations of materials with different densities and sharp interfaces.

29 March 2024, 19:41:53

The 3D-printed layered material showed critical detonation diameters significantly larger than those of corresponding homogenous PBX with the same Al content. The layered materials also are less prone to ignition under impact, therefore, are less sensitive and safer. Complex patterns of cavities have also been created in materials. Yang *et al.*²⁴ used a SLA method to introduce 2 mm pores in an energetic material with 50 wt. % of RDX. The void creation during the AM process takes advantage of controlled processing parameters. For example, voids around 100 μm in diameter can be created during inkjet printing.²⁵ Obviously, graded materials can be produced by varying the process parameters.

In this paper, we focus on materials with gradients of void density, and use the study to explore and demonstrate the potential of FGEM. A fully 3D microstructure-explicit model for PBX is used to simulate the shock to detonation transition (SDT) process. Five material cases are used to delineate the effect of void gradient. Two cases involve graded distribution of voids along the length of the sample. These two cases use the same samples, with each sample impacted from the two different ends, thereby entailing the shock wave propagating from both the high material density (low void fraction) end to the low material density (high void fraction) end and vice versa. The other three cases involve uniform distributions of voids (no gradient). These three cases act as a baseline for comparison to delineate the effect of the void gradient and to illustrate that the graded samples can yield behaviors not obtainable by samples without gradients. Our quantification focuses on the run-to-detonation distance (RDD) as well as the time duration of the SDT process and the change in the shock front velocity associated with the SDT.

II. FRAMEWORK OF ANALYSIS

The 3D simulations are carried out using the CTH hydrocode. Sustained loading is affected on the sample via the use of a thick aluminum flyer 6 mm in length, with velocities varying from 600 to 1200 m/s, resulting in shock pressures between 4 and 8 GPa. In Sec. II A, the method for generating 3D microstructure samples is discussed. An outline of the constitutive models used is given in Sec. II B.

A. Material, model, and microstructure

The focus of this study is on PBX configurations HMX and Estane which track the overall characteristics of PBX9501. For HMX, we use an Arrhenius reaction model. These materials were chosen based on readily available material model parameters, the desire to compare the influence of different models on the study of the gradient effects, and the chance to compare the computational results with available experimental data of the run distance for PBX9501. The constituents of these materials are commonly used in a variety of energetic materials.^{26–28} The microstructure grain-binder morphology is generated through Voronoi tessellation. This method has been described in previous publications,^{4,11} so will not be discussed here. This random microstructure sample is $6 \times 1 \times 1 \text{ mm}^3$ in size and has an average grain size of 150.5 μm , grain size standard deviation of 68 μm , and grain volume fraction of 75%.^{29–31}

The microstructure is overlaid with five different void distributions as shown in Fig. 2 for a total of five material cases. Two of the cases contain a linear void gradient along the 6 mm length of the sample, from 1% to 10% void fraction (high material density to low material density, HL) and vice versa (LH). This results in a void volume fraction gradient of $\pm 1.5\%/ \text{mm}$ for LH and HL, respectively, or a material density gradient of $\pm 0.026 \text{ g}/(\text{cm}^3 \text{ mm})$. These two gradient cases use the same void distribution in the microstructure. The difference is in how the sample is used in the analysis or which end is subjected to impact loading: the low material density (high void fraction) end or high material density (low void fraction) end. The case of impact at the 1% void end (high material density) is denoted as **HL**, as the shock wave travels from high material density into low material density. Conversely, the case of impact at the 10% void case is denoted **LH**, as the shock wave travels from low material density into low material density. Thus, each sample can have multiple uses or functionalities. The three remaining void distributions are uniform (no gradient) with volume fraction of 1% (high material density), 5.5% (average material density), and 10% (low material density), labeled as **HH**, **MM**, and **LL**, respectively. The uniform cases serve as a baseline for understanding the effects of void gradients through comparison. The combination of graded and non-graded samples also allows the question “can graded samples yield detonation behaviors (e.g., run distance, SDT transition time, shock front velocity increase over SDT) that are unobtainable by uniform samples” to be answered. The voids are spheres 50 μm in diameter. This size is larger than the size of most experimentally reported voids and is necessitated by the need for computational efficiency and the millimeter size scale of the 3D models. It allows the trend in material behavior to be explored.³²

B. Constitutive relations

The mechanical behavior of the HMX grains is described with a simplified Steinberg–Guinan–Lund (SGL) strain dependent flow stress model. This strain-rate dependent model is well-suited for high strain-rate deformation and accounts for the effects of thermal softening. The material flow stress is calculated via

$$\sigma_Y(\dot{\epsilon}_P, T) = [\sigma_A + \sigma_T(\dot{\epsilon}_P, T)], \quad (1)$$

with

$$\dot{\epsilon}_P = \left\{ \frac{1}{C_1} \exp \left[\frac{2U_K}{T} \left(1 - \frac{\sigma_T}{\sigma_P} \right)^2 \right] + \frac{C_2}{\sigma_T} \right\}^{-1}. \quad (2)$$

In the above relations, σ_A (MPa) is the thermal component of the flow stress, σ_T (MPa) is the thermally activated component of the flow stress, and C_1 (1/s), C_2 (Pa s), U_K (K), and σ_P (MPa) are material parameters. The parameters used are taken from previous works.⁴

The binder uses by an elastic perfectly plastic flow stress model based on the von Mises yield surface concept called EPPVM. This model captures the effects of thermal softening and density degradation under shock loading. The yield surface is given

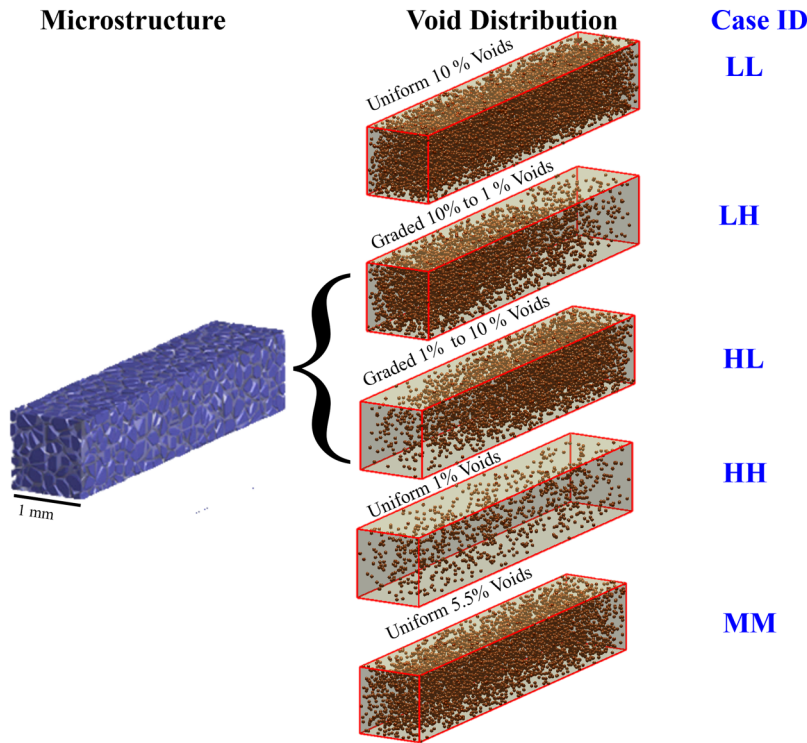


FIG. 2. Three-dimensional microstructure sample set containing void distributions. The same microstructure grain-binder morphology is used. The five void distributions are uniform low material density **LL**, graded material density from low material density to high material density **LH**, graded material density from high material density to low material density **HL**, uniform high material density **HH**, and uniform average material density **MM**.

by

$$Y = \begin{cases} \sigma_y & \text{if } T < T_{melt}, \\ \frac{(T - T_{melt})(\alpha - 1)}{T_{melt}} \sigma_y & \text{if } T \geq T_{melt}. \end{cases} \quad (3)$$

In the above expressions, Y (MPa) is the current flow stress or yield strength of the material, T (K) is the temperature, and α is equal to ρ_0/ρ , with ρ (g/cm³) being the current density and ρ_0 (g/cm³) being the reference density.

The first-order Mie Grüneisen equation of state (MGEOS) is used to describe the bulk response of the grains in the solid phase, i.e.,

$$p = \frac{\rho_0 C_0^2 \left(1 - \frac{\rho_0}{\rho}\right) \left[1 - \frac{\Gamma_0}{2} \left(1 - \frac{\rho_0}{\rho}\right)\right]}{\left[1 - s \left(1 - \frac{\rho_0}{\rho}\right)\right]^2} + \Gamma_0 E. \quad (4)$$

Here, p is the pressure, Γ_0 is the Grüneisen parameter, C_0 (m/s) is the bulk sound speed, and s is the slope of the Hugoniot. E is the internal energy per unit volume which can be determined by integrating the specific heat with respect to temperature at constant

volume, i.e.,

$$E = \frac{1}{V_0} \int_0^T c_v dT. \quad (5)$$

The parameters for the MGEOS used for HMX are taken from available data.³³ The HMX reaction product EOS is described by tabular data.³³

C. Chemical kinetics

The Arrhenius Reactive Burn (ARB) chemical kinetics model is used to track the rate of chemical reaction in the PETN grains. This empirical model more accurately tracks the development of local field variables, such as temperature and pressure rise due to chemical reaction, than other burn models, such as the History Variable Reactive Burn (HVRB).²⁹ The ARB model tracks the rate of chemical reaction in the HMX using the form

$$\begin{aligned} d\lambda/dt &= \begin{cases} (1 - \lambda)F \exp(-\Theta/T) & \text{if } T \geq T_i, \\ 0 & \text{if } T < T_i, \end{cases} \quad \text{with } \Theta \\ &= \Theta_0(1 + A_p P). \end{aligned} \quad (6)$$

In the above relations, λ is the fraction of reacted material, t (s) is the time, T (K) is the temperature, F (1/s) is a pre-exponential frequency factor, Θ_0 (K) is the activation temperature of the material, A_p (1/MPa) is a parameter quantifying the pressure

dependence of the reaction rate, and P (MPa) is the pressure. T_i (K) indicates the threshold temperature below which the reaction rate is zero. The parameters for the ARB model for pure HMX crystals are taken from Kerley³⁴ and Springer *et al.*³⁵ To explore how the ARB model parameter influence the SDT behavior of the materials and to obtain parameter values that lead to better matches with experimentally measured run distance datasets, a parametric study is carried out by varying the value of F . This analysis allows a set of values to be obtained here to better describe the behavior of PBX9501 batches studied in several previous publications by different authors.

D. Mesh convergence

To ensure that accurate RDD and pressure values are obtained, a mesh convergence study has been performed. The measures of focus for the mesh convergence study are the RDD and the pressure. Element sizes ranging from 50 to 5 μm are used. The mesh convergence study was performed using the HH microstructure case. It is found that elements 10 μm and smaller provide consistent and converging results in both the RDD and pressure.⁴ Therefore, an element size of 10 μm is chosen as it allows for increased computational efficiency as well as sufficient resolution of the voids.

III. RESULTS

A systematic quantification of the effect of the void gradient on the SDT behaviors of the HMX/ESTANE (PBX9501) composite is carried out. Section III A discusses the SDT process as measured by its time duration and associated increase in shock front velocity. Section III B covers the Pop plot and the effect void gradients have. Section III C focuses on the change in shock front velocity, time duration, and distance associated with the SDT process.

A. Shock to detonation transition process and run distance

A heterogeneous shock to detonation transition process is observed, as shown in Fig. 3 for a HL sample with an impact velocity of 1100 m/s (shock pressure 4.9 GPa). Figure 3(a) displays the pressure distributions at three distinct times of the SDT process. The variations of the average pressure along the sample length at the same times are shown in Fig. 3(b). Initially, mechanical loading

is seen without appreciable chemistry [Fig. 3(a), position 1, 310 ns] where the pressure is evenly distributed in the shocked material [Fig. 3(b), position 1]. As the shock wave moves through the material, inelastic dissipation leads to hotspots and the initiation of chemistry [Fig. 3(a), position 2, 650 ns]. The chemical reactions lead to a pressure rise within the material near the shock front [Fig. 3(b), position 2]. The evolution of chemistry eventually causes the shock front to become a detonation front traveling at a higher speed with a much higher pressure [Fig. 3(a), position 3, 970 ns]. The detonation front has a sharp pressure peak between the shocked and unshocked materials [Fig. 3(b), position 3]. The distance traversed by this time is defined as the run-to-detonation distance (RDD), also shown in Fig. 3(a), position 3. We characterize the RDD as when the detonation front reaches a constant velocity higher than the shock velocity. The method previously developed by Miller *et al.* and used by Miller *et al.*⁴ and Coffelt *et al.*¹¹ is used here for the calculation. For the case in Fig. 3, RDD = 4.54 mm.

B. Effect of void gradient on the Pop plot

The Pop plot (RDD as a function of applied shock pressure) for the five material cases is shown in Fig. 4, with Fig. 4(a) showing the result using the ARB parameters from Kerley³⁴ and Springer *et al.*³⁵ and Fig. 4(b) showing the result by changing the value of the frequency factor F from 5.6×10^{12} 1/s to 2.5×10^{12} 1/s in order to obtain a better fit to experimental data reported in the literature. Note that the plots use log-log scales. Overall, the lines represent power-law fit to each data set. The specific power law used for the fit is^{4,11,36}

$$x = SP^m, \quad (7)$$

where x is the run distance, P is the pressure, and $S(\text{GPa}^m \text{ mm})$ and m are fitting parameters, whose values are shown in Table I. The effects of void distribution can be clearly seen. The three uniform cases (HH, MM, and LL) follow the expected trend where increasing the amount of voids increases the material sensitivity (lower run distance values). The gradient cases (HL and LH) show RDD levels and trends that are different from the uniform cases. First, note that these two cases show distinctively different Pop plot lines, with the line for HL close to but below the line for HH and much higher than the line for LH. This difference occurs even though the two cases involve the same samples, only that they are impacted

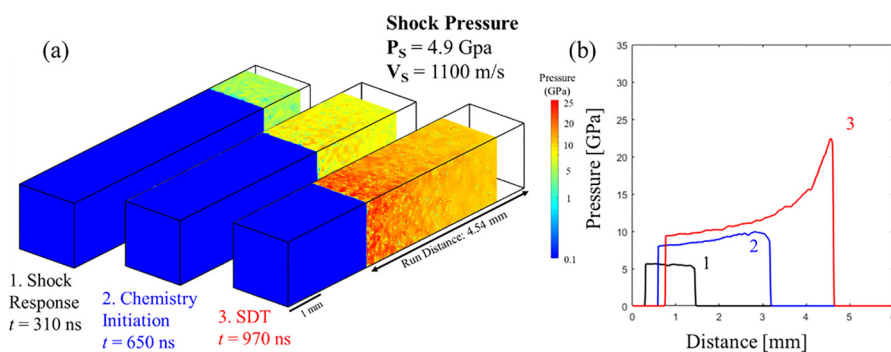


FIG. 3. The shock to detonation transition process of a HL sample impacted with a velocity of 1100 m/s. The shock pressure is 4.9 GPa. (a) Distributions of pressure at three different times corresponding to different stages. (b) Profiles of average pressure along the sample length at the three stages shown in (a).

29 March 2024, 19:41:53

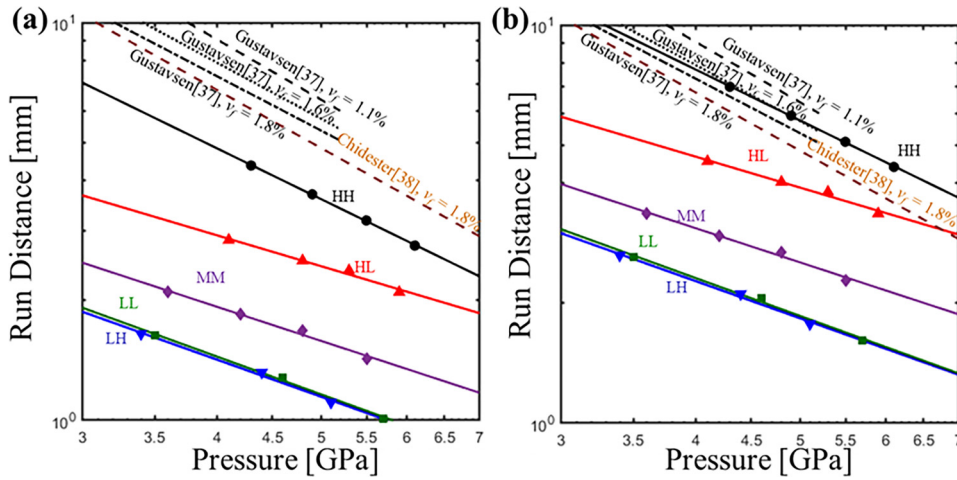


FIG. 4. Run-to-detonation distance (RDD) as a function of shock pressure (Pop plot) for the five cases analyzed. (a) Calculations using the HMX frequency factor $F = 5.6 \times 10^{12}$ 1/s found in the literature and (b) calculations using $F = 2.5 \times 10^{12}$ 1/s for better match with experiments of different volume fractions (v_f) from Gustavsen *et al.* (black line)³⁷ and Chidester *et al.* (brown line).³⁸ From highest to lowest RDD on average: uniform high material density (HH), gradient high to low material density (HL), uniform average material density (MM), gradient low to high material density (LH), and uniform low material density (LL).

from opposite ends. Therefore, graded samples are macroscopically anisotropic such that different behaviors can be obtained via loading in different directions. Second, note that the HL and LH samples have an average void fraction of 5.5% which is the same as that of the MM sample. However, the two graded cases have very different Pop plot lines from that of the MM case. Consequently, graded samples can be used to obtain RDDs significantly different from those of uniform samples of the same weight (material density), thereby expanding the range of PBX performance via microstructure modification without change in the amount of material used or overall sample weight. Additionally, note also that the HL Pop plot line cannot be obtained by uniform sample of any density, although the LH line is quite similar to the line for LL. So, overall, graded samples significantly expand the range of possible behavior outcome of PBX. Note also that the slopes (quantified by m) of the Pop plot lines for the different cases are also different, even among the uniform density cases (HH, MM, and LL). Since the slope relates to the dependence of the RDD on pressure, the result shows that microstructure gradient can also be used to alter the slope m of the Pop lines or the rate of change of RDD as a function of input pressure. In particular, a decreasing material density (negative gradient, HL, slope $m = -0.80$, Table I) can be used to decrease the slope relative to HH (slope $m = -1.32$, Table I) of the Pop plot line. On the other hand, the data show that an increasing material density (positive gradient, LH, slope $m = -0.97$) does not appreciably change the slope relative to the LL case (slope $m = -0.98$). Due to the limited amount of data here, more analyses

are needed to more definitively characterize and explain the trend in the slopes.

To obtain the better match with the experimental data shown in Fig. 4(b), the HH case is used to calibrate the ARB model by changing the frequency factor F , as this case has a void volume fraction of 1% which is similar to the void volume fraction in the experimental data sets. This study begins by noting that the RDD line in Fig. 4(a) is lower than the experimentally measured lines for a similar void density. The parametric study involves a systematic variation of F . As the slopes of the lines are already similar, the focus is on reducing the rate of the reaction by decreasing frequency factor F . It is found that a reduction of F by roughly half, from 5.6×10^{12} 1/s to 2.9×10^{12} 1/s, increases the run distance by 1.14 mm on average. This leads to an estimate value of 2.5×10^{12} 1/s which yields the calculated RDD line for HH shown in Fig. 4(b). Subsequently, the RDD lines for HL, MM, LH, and LL are calculated accordingly and shown in Fig. 4(b). It should be noted that the trends seen in Tables I and II are not overly affected by the change in F .

Table II shows the average vertical decrease in lines fitted to the RDD relative to the HH case. HL shows RDDs that are on average 25.49% lower than the corresponding values for HH. The average RDDs for LH, LL, and MM are 68.39%, 68.31%, and 55.23%, respectively, lower relative to the HH case. Again, the data show that void density gradient, just like void density itself, can be used to significantly alter or tailor the Pop plot of the PBX and obtain results not obtainable from uniform samples without gradients.

TABLE I. Effect of void distribution on the slopes of the fitted Pop plot curves.

Material case	S (GPa ^m mm)	M
HH	29.96	-1.32
HL	8.89	-0.80
MM	6.61	-0.89
LH	5.4124	-0.97
LL	5.6491	-0.98

TABLE II. Effect of void distribution on normalized run distance for 3D samples.

Void distribution	Average decrease in RDD relative to HH (%)
HH	0
HL	25.49
MM	55.23
LH	68.39
LL	68.31

29 March 2024, 19:41:53

$$V = 1300 \text{ m/s}, P_s = \sim 6 \text{ GPa}, t = 440 \text{ ns}$$

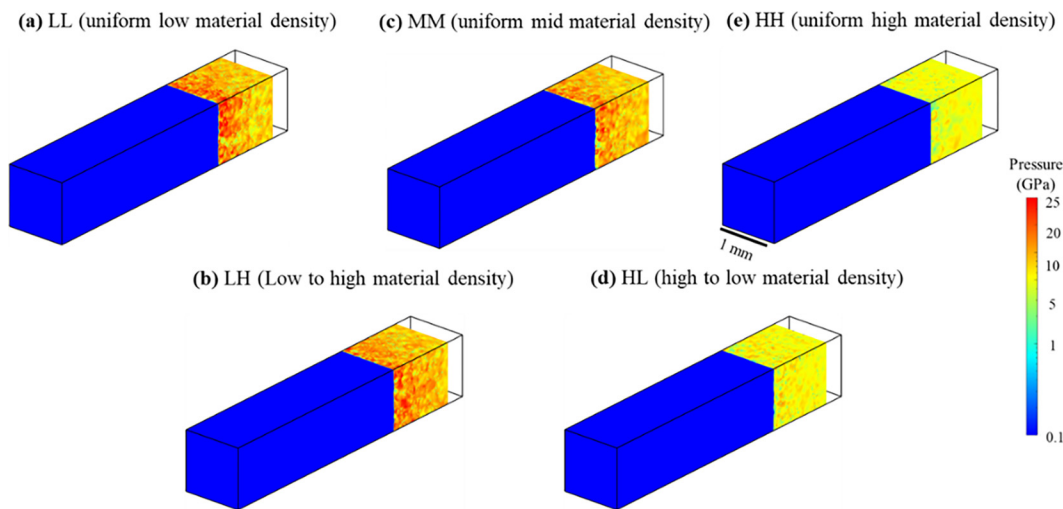


FIG. 5. A comparison of the pressure distributions for the five materials' cases under a shock pressure around 6 GPa at a time before any case has reached detonation. (a) Uniform low material density (LL), (b) gradient low to high material density (LH), (c) uniform average material density (MM), (d) gradient high to low material density (HL), and (e) uniform high material density (HH).

To help understand the underlying mechanism for the difference in behavior, Fig. 5 shows the pressure distributions in a sample from each material case at $t = 440 \text{ ns}$ for the impact velocity of 1300 m/s. This time is before any material has reached detonation. The pressure is higher in the LL, LH, and the MM cases than in HH and HL. Clearly, higher void content near the impacted end facilitates the initiation of chemical reaction which leads to earlier ignition, hotspot development, and local pressure increase, resulting in eventual earlier SDT (lower RDD). The result again shows that void gradient offers another means to manipulate the ignition and detonation behavior of energetic materials.

C. Time and spatial durations of the SDT process and increase in shock front velocity

Where and how fast SDT is achieved can also be useful measures for the behavior of energetic materials. Similarly, the acceleration or the increase in the velocity of the shock front associated with the SDT is of interest. Here, these quantities are studied to further delineate the effects of void distribution. It is understood that the shock velocity and detonation velocity are dependent on material density.^{39, 40} Figure 6 shows, for the five material cases, (a) the time history of the shock front position and (b) and (c) the shock front velocity as a function of time and distance. The impact velocity is 1300 m/s. The run distance can be determined from the profiles as well. Note that the profiles reflect a degree of smoothing in the numerical differentiation and curve fitting.

The transition from shock to detonation entails a clearly defined time or position at which the shock front begins to accelerate (front velocity begins to increase). The completion of the SDT

is marked by an instantaneous jump in the velocity to a final plateau value. The interest here is not on the final plateau detonation velocity value, but rather on the amount of increase in the shock front velocity up to the point before the jump occurs, which is denoted as Δv , as seen in Figs. 6(b) and 6(c). The increase is used along with the time duration of SDT (time different between SDT onset and SDT completion), Δt in Fig. 6(b). The distance over which the SDT plays out is denoted as Δd , as seen in Fig. 6(c). The cases with lower material density levels at the impacted end (i.e., LL, LH, and MM) display shorter Δt . This result is not unexpected. Lower material density (higher void fraction) at the impact end leads to earlier reaction initiation and faster hotspot development, as shown above. In contrast, the lower amounts of voids near the impact end for the HL and HH cases leads to later onset and longer durations of SDT.

An analysis of Δt , Δd , and Δv as a function of shock pressure is shown in Figs. 7(a)–7(c). The uniform high material density case, HH, has the longest time and spatial durations (Δt and Δd) and the lowest shock front velocity increase and acceleration (Δv and $\Delta v/\Delta t$), representing the least sensitive case. This is unsurprising, as fewer voids correspond to lower chances of temperature pressure increases associated with void collapse. We use this as a baseline case for comparison. The other four cases are close to each other or have overlap in all four measures; however, trends can be discerned. Specifically, HL is the next least sensitive material, with lower Δt and Δd and higher Δv and $\Delta v/\Delta t$ relative to HH. Note that LH is more sensitive than HL, with lower Δt and Δd and higher Δv and $\Delta v/\Delta t$ than HL. Clearly, the same graded specimen can be used to obtain different shock and SDT behaviors by impacting from different ends. This is what is referred to as

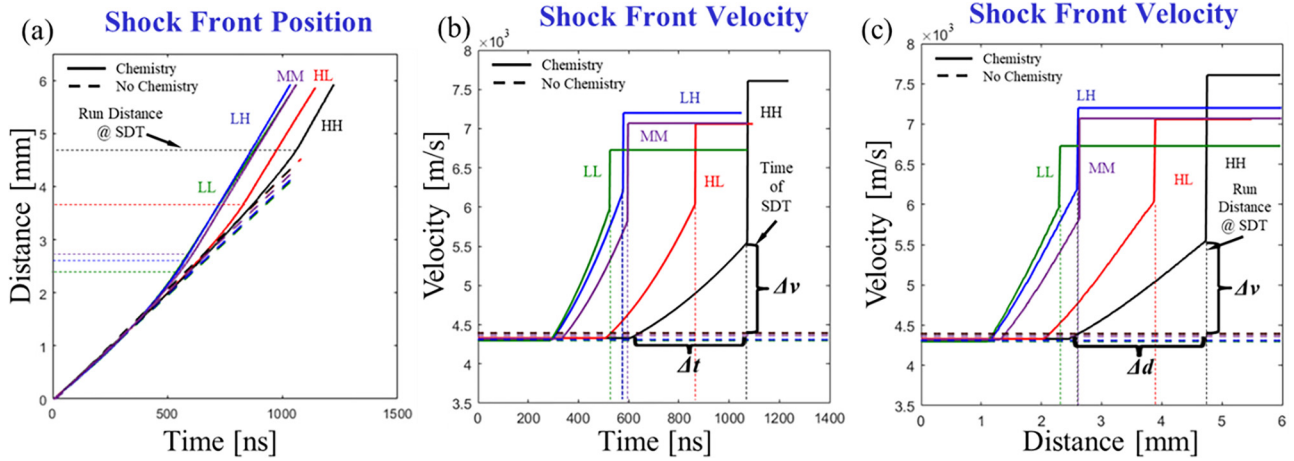


FIG. 6. The SDT process as measured by (a) the position of the shock front in the material through time, (b) the time derivative of (a) or the shock front propagation velocity as a function of time, and (c) the derivative of (a) or the shock front propagation velocity as a function of distance. The distances and times of SDT start and completion are clearly outlined.

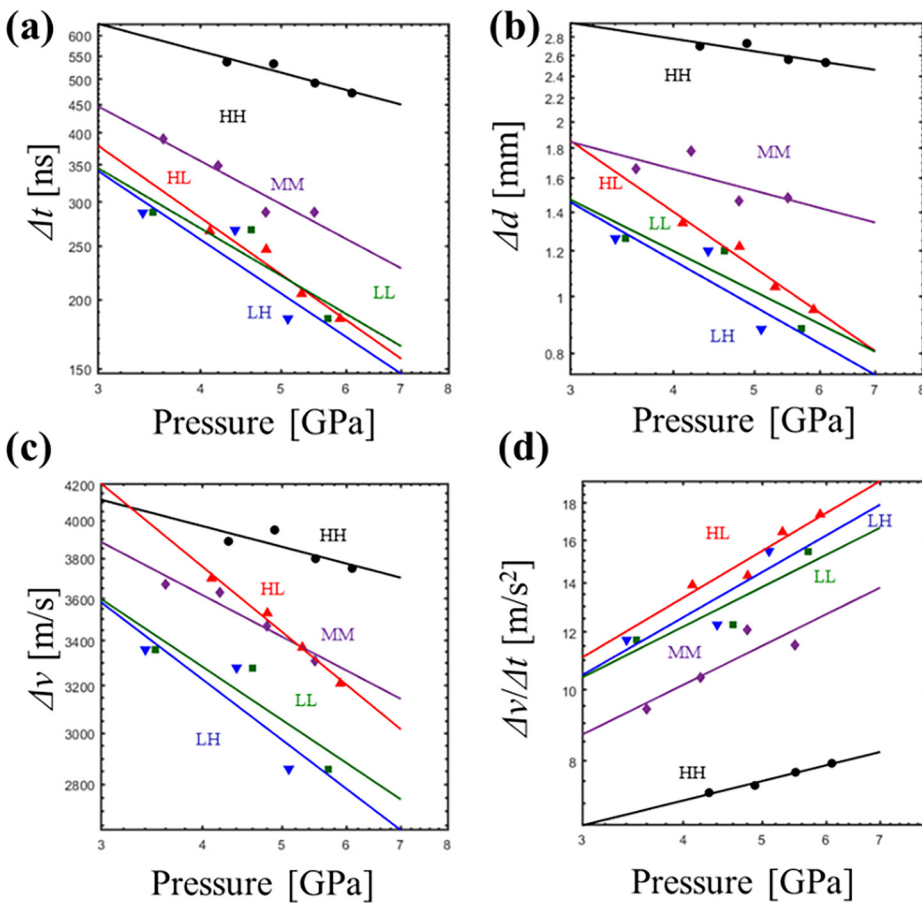


FIG. 7. (a) SDT time duration Δt as a function of shock pressure, (b) SDT distance Δd as a function of shock pressure, (c) shock front velocity increase Δv as a function of shock pressure, and (d) shock front acceleration $\Delta v/\Delta t$ as a function of shock pressure.

29 March 2024 19:41:53

multifunctionality of a material sample. Although MM (uniform sample with the average density of the HL and LH graded sample) shows behaviors close to that of LH, the overall slopes of the pressure dependence for Δt , Δd , and $\Delta v/\Delta t$ are slightly different and the overall levels of Δv is lower than those of HL, suggesting that the graded cases have aspects of behaviors that cannot be produced by uniform (non-graded) samples. The clearest indication of this is that the shock front velocity increase over SDT (Δv) in Fig. 7(c) clearly distinguishes the cases from each other. Overall, LL is the most sensitive case [shortest time and spatial durations (Δt and Δd)] and the highest shock front acceleration ($\Delta v/\Delta t$); however, its shock front velocity increase (Δv) falls below those of LH and MM.

It is worth noting that the simulations have used the Arrhenius reactive burn model (ARB). There is a need to compare how different material models would affect the results. We are carrying out such a study and will report the outcome in a future publication.

IV. CONCLUSION

There has been significant study on the effect of heterogeneities on the ignition and detonation behaviors of energetic materials. It is well known that increasing the density of heterogeneities increases the sensitivity of an energetic material to shock loading. To expand microstructure attribute space for designing materials with wider ranges of behavior outcomes, we have used the concept of Functionally Graded Energetic Materials (FGEMs) which have spatially non-uniform or graded microstructure heterogeneities. These materials use controlled changes in the microstructure, such as void and grain density and/or size changes, to alter the ignition and detonation behaviors of the materials. As specific case studies in this paper, we have focused on microstructure configurations involving a spatial gradient of void density along the length of the sample (specifically, changes in volume fraction between 1% and 10% over a length of 6 mm). Calculations recognize the macroscopic directional anisotropy of the graded samples by considering shock loading from different directions of the macroscopically asymmetric samples. For comparison, three uniform cases at representative void volume fractions of 1%, 5.5%, and 10% are also analyzed. The results show that the gradient cases exhibit SDT behaviors that depend on both the magnitude and sign of the void gradient. Specifically, loading from the opposite ends of the same graded sample [i.e., different signs (positive or negative) of gradient] yields totally different results. Additionally, the magnitude of the gradient (graded or non-graded) also significantly affects the behavior. More interestingly, the behaviors of some graded cases cannot be obtained by non-graded samples of any void density. Clearly, the results here show that spatial gradient of voids can be used to design new energetic materials with responses existing materials do not offer. A parametric study has allowed material model parameters to be obtained to provide calculated Pop plot trends that closely match experimentally measured Pop plot data sets in the literature.

As indicated in Fig. 1, many different microstructure attributes can be involved in designing FGEM, including but not limited to grain size/density, void size/density, metal particle size/density, and sharp interfaces. We have only considered gradients in voids in this

paper, with the hope that this can excite more studies. Future analyses, both computational and experimental, can focus on gradients in other attributes not analyzed here.

ACKNOWLEDGMENTS

Support from Los Alamos National Lab through LANL sub-contract No. 633534 (Dr. Von Howard Whitley) is sincerely acknowledged.

AUTHOR DECLARATIONS

Conflict of Interest

The authors have no conflicts to disclose.

Author Contributions

Daniel Olsen: Data curation (equal); Investigation (equal); Methodology (equal); Writing – original draft (equal). **Min Zhou:** Conceptualization (equal); Methodology (equal).

DATA AVAILABILITY

The data that support the finding of this study are available from the corresponding author upon reasonable request.

REFERENCES

- ¹F. P. Bowden, A. D. Yoffe, and G. E. Hudson, "Initiation and growth of explosion in liquids and solids," *Am. J. Phys.* **20**(4), 250–251 (1952).
- ²M. A. Wood, M. J. Cherukara, E. M. Kober, and A. Strachan, "Ultrafast chemistry under nonequilibrium conditions and the shock to deflagration transition at the nanoscale," *J. Phys. Chem.* **119**(38), 22008–22015 (2015).
- ³M. R. Baer, "Modeling heterogeneous energetic materials at the mesoscale," *Thermochim. Acta* **384**, 351–367 (2002).
- ⁴C. Miller, D. Olsen, Y. Wei, and M. Zhou, "Three-dimensional microstructure-explicit and void-explicit mesoscale simulations of detonation of HMX at millimeter sample size scale," *J. Appl. Phys.* **127**(12), 125105 (2020).
- ⁵J. Ramsay and A. Popolato, *Analysis of Shock Wave and Initiation Data for Solid Explosives* (Los Alamos Scientific Laboratory, University of California, Albuquerque, NM, 1965).
- ⁶B. A. Khasainov, B. S. Ermolaev, H.-N. Presles, and P. Vidal, "On the effect of grain size on shock sensitivity of heterogeneous high explosives," *Shock Waves* **7**(2), 89–105 (1997).
- ⁷S. M. Walley, J. E. Field, and M. W. Greenaway, "Crystal sensitivities of energetic materials," *Mater. Sci. Technol.* **22**(4), 402–413 (2006).
- ⁸S. Zeman and M. Jungová, "Sensitivity and performance of energetic materials," *Propellants Explos. Pyrotech.* **41**(3), 426–451 (2016).
- ⁹J. Zhang and T. L. Jackson, "Effect of microstructure on the detonation initiation in energetic materials," *Shock Waves* **29**(2), 327–338 (2019).
- ¹⁰M. Baer, M. Kipp, and F. Van Swol, "Micromechanical modeling of heterogeneous energetic materials," No. SAND-98-1945C; CONF-980803, Sandia National Laboratories, 1998.
- ¹¹C. Coffelt, D. Olsen, C. Miller, and M. Zhou, "Effect of void positioning on the detonation sensitivity of a heterogeneous energetic material," *J. Appl. Phys.* **131**(6), 065101 (2022).
- ¹²B. Olinger, *Compacting Plastic-Bonded Explosive Molding Powders to Dense Solids* (Los Alamos National Lab, Los Alamos, NM, 2005).
- ¹³J. S. Gharia, A. S. Kumar, L. N. Raghavendra, and S. R. Vadali, "Effect of density gradient and porosity on HMX/TNT pressure cast shaped charge performance," *Propellants Explos. Pyrotech.* **21**(1), 36–39 (1996).

- ¹⁴W. B. Zhang, H. Huang, Y. Tian, and B. Dai, "Characterization of RDX-based thermosetting plastic-bonded explosive by cone-beam microfocus computed tomography," *J. Energy Mater.* **30**(3), 196–208 (2012).
- ¹⁵J. D. Yeager, V. W. Manner, J. A. Stull, D. J. Walters, A. M. Schmalzer, D. J. Luscher, and B. M. Patterson, "Importance of microstructural features in mechanical response of cast-cured HMX formulations," in *AIP Conference Proceedings* (AIP Publishing, 2018).
- ¹⁶R. E. Hollands and I. E. P. Murray, "BAE systems," PLC CA 2735320C, 2010.
- ¹⁷H. A. Bruck, F. M. Gallant, and S. Gowrisankaran, "Development of a novel continuous processing technology for functionally graded composite energetic materials using an inverse design procedure," in *Proceedings of the 2002 SEM Annual Conference & Exposition* (Springer/SPI-global, 2002), p. 296.
- ¹⁸N. V. Muravyev, K. A. Monogarov, U. Schaller, I. V. Fomenkov, and A. N. Pivkina, "Progress in additive manufacturing of energetic materials: Creating the reactive microstructures with high potential of applications," *Propellants Explos. Pyrotech.* **44**(8), 941–969 (2019).
- ¹⁹J.-C. Zhang, K. He, D.-W. Zhang, J.-D. Dong, B. Li, Y.-J. Liu, G.-L. Gao, and Z.-X. Jiang, "Three-dimensional printing of energetic materials: A review," *Energ. Mater. Front.* **3**(2), 97–108 (2022).
- ²⁰B. Huang, Z. Xue, X. Fu, and Q.-L. Yan, "Advanced crystalline energetic materials modified by coating/intercalation techniques," *Chem. Eng. J.* **417**, 128044 (2021).
- ²¹A. K. Murray, T. Isik, V. Ortalan, I. E. Gunduz, S. F. Son, G. T.-C. Chiu, and J. F. Rhoads, "Two-component additive manufacturing of nanothermite structures via reactive inkjet printing," *J. Appl. Phys.* **122**(18), 184901 (2017).
- ²²A. K. Murray, W. A. Novotny, T. J. Fleck, I. E. Gunduz, S. F. Son, G. T.-C. Chiu, and J. F. Rhoads, "Selectively-deposited energetic materials: A feasibility study of the piezoelectric inkjet printing of nanothermites," *Add. Manuf.* **22**, 69–74 (2018).
- ²³X. Zhou, Y. Mao, D. Zheng, L. Zhong, R. Wang, B. Gao, and D. Wang, "3D printing of RDX-based aluminized high explosives with gradient structure, significantly altering the critical dimensions," *J. Mater. Sci.* **56**, 9171–9182 (2021).
- ²⁴W. Yang, R. Hu, L. Zheng, G. Yan, and W. Yan, "Fabrication and investigation of 3D-printed gun propellants," *Mater. Design* **192**, 108761 (2020).
- ²⁵C. O'Grady, M. P. Marquez, S. Rupper, J. Vasiliauskas, R. Knepper, S. F. Son, and A. S. Tappan, "Investigating typical additive manufacturing defect geometries using physical vapor deposition explosives as a model system," in *21st Biennial Conference of the APS Topical Group on Shock Compression of Condensed Matter, Portland, OR, 16–21 June* (AIP Publishing, 2020), Vol. 64.
- ²⁶S. Chaturvedi and P. N. Dave, "Solid propellants: AP/HTPB composite propellants," *Arabian J. Chem.* **12**(8), 2061–2068 (2019).
- ²⁷K.-S. Jaw and J.-S. Lee, "Thermal behaviors of PETN base polymer bonded explosives," *J. Therm. Anal. Calorim.* **93**(2008), 953–957 (2008).
- ²⁸S. J. P. Palmer, J. E. Field, and J. M. Huntley, "Deformation, strengths and strains to failure of polymer bonded explosives," *Proc. R Soc London Ser. A* **440**(1909), 399–419 (1993).
- ²⁹C. Miller, D. Kittell, C. Yarrington, and M. Zhou, "Prediction of probabilistic detonation threshold via millimeter-scale microstructure-explicit and void-explicit simulations," *Propellants Explos. Pyrotech.* **45**, 254–269 (2020).
- ³⁰Y. Wei, S. Kim, Y. Horie, and M. Zhou, "Quantification of probabilistic ignition thresholds of polymer-bonded explosives with microstructure defects," *J. Appl. Phys.* **124**(16), 165110 (2018).
- ³¹Y. Wei, C. Miller, D. Olsen, and M. Zhou, "Prediction of probabilistic shock initiation thresholds of energetic materials through evolution of thermal-mechanical dissipation and reactive heating," *J. Appl. Mech.* **88**, 091005 (2021).
- ³²T. M. Willey, L. Lauderbach, F. Gagliardi, T. van Buuren, E. A. Glascoe, J. W. Tringe, J. R. Lee, H. K. Springer, and J. Ilavsky, "Mesoscale evolution of voids and microstructural changes in HMX-based explosives during heating through the β - δ phase transition," *J. Appl. Phys.* **118**, 055901 (2015).
- ³³E. S. Hertel and G. I. Kerley, "CTH EOS package: Introductory tutorial," Sandia National Laboratories Report SAND98-0945, Sandia National Laboratory (SNL-NM), 1998.
- ³⁴G. I. Kerley, *Hydrocode Calculations of Detonator/Booster Initiation by Fragment Impacts* (Sandia National Laboratory (SNL-NM), Albuquerque, NM, 1997), pp. 1–50.
- ³⁵H. K. Springer, S. Bastea, A. L. Nichols III, C. M. Tarver, and J. E. Reaugh, "Modeling the effects of shock pressure and pore morphology on hot spot mechanisms in HMX," *Propellants Explos. Pyrotech.* **43**(8), 805–817 (2018).
- ³⁶R. Menikoff, *Review of PBX 9502 Pop Plot Data* (Los Alamos National Lab, Los Alamos, NM, 2018).
- ³⁷R. Gustavsen, S. Sheffield, R. Alcon, and L. Hill, "Shock initiation of new and aged PBX 9501," in *Twelfth International Detonation Symposium, Arlington, VA* (Office of Naval Research, 2002), p. 530.
- ³⁸S. K. Chidester, D. G. Thompson, K. S. Vandarsall, D. J. Idar, C. M. Tarver, F. Garcia, and P. A. Urtiew, "Shock initiation experiments on PBX 9501 explosive at pressures below 3 GPa with associated ignition and growth modeling," *AIP Conf. Proc.* **955**, 903 (2007).
- ³⁹V. V. Sil'vestrov, "Density dependence of detonation velocity for some explosives," *Combust. Explos. Shock Waves* **42**, 472–479 (2006).
- ⁴⁰S. Kubota, T. Saburi, Y. Ogata, and K. Nagayama, "Estimation of initial state dependence of detonation velocity using unified form of EOS for PETN," *Mater. Sci. Forum* **767**, 28 (2013).